Imtiaz, A., Causse, M., Chaljub, E., Cotton, F. (2015): Is Ground-Motion Variability Distance Dependent? Insight from Finite-Source Rupture Simulations. - *Bulletin of the Seismological Society of America*, *105*, 2A, p. 950-962.

DOI: http://doi.org/10.1785/0120140107

Bulletin of the Seismological Society of America, Vol. 105, No. 2A, pp. 950–962, April 2015, doi: 10.1785/0120140107

Is Ground-Motion Variability Distance Dependent? Insight from Finite-Source Rupture Simulations

by Afifa Imtiaz, Mathieu Causse, Emmanuel Chaljub, and Fabrice Cotton*

Abstract The ground-motion variability sigma is a fundamental component in probabilistic seismic-hazard assessment because it controls the hazard level at very low probabilities of exceedance. So far, most of the analyses based on empirical ground-motion prediction equations do not consider any distance dependency of sigma. This study aims to analyze the potential distance dependency of ground-motion variability, especially in the near-field region, where the variability is poorly constrained due to the lack of available records. We, therefore, investigate the distance dependency of sigma by performing numerical simulations of ground motion for some strike-slip events. Synthetic velocity seismograms (up to 3 Hz) have been generated from a suite of finite-source rupture models of past earthquakes. Green's functions were calculated for a 1D velocity structure using a discrete wavenumber technique (Bouchon, 1981). The within-event component of the ground-motion variability was then evaluated from the synthetic data as a function of distance. The simulations reveal that the within-event component of the ground motion shows a distance dependency, subject to the rupture type. For bilateral ruptures, the variability tends to increase with distance. On the contrary, in case of unilateral events, the variability decreases with distance.

Introduction

Empirical ground-motion prediction equations (GMPEs) developed by means of regression techniques from recorded strong-motion data, generally are based on very simple parameterization with magnitude (**M**), distance (d), and site category (s). The distribution of ground motion for a given **M**, d, and s is then represented in terms of a median and a standard deviation, referred to as the aleatory variability sigma, which is a fundamental component in probabilistic seismic-hazard analysis (PSHA). Sigma exerts a strong influence on the seismic-hazard level, especially for long return periods (Bommer and Abrahamson, 2006). It is therefore imperative to accurately constrain sigma to perform reliable seismic-hazard analyses.

In seismic-hazard studies two types of uncertainties, termed as aleatory variability and epistemic uncertainty, are considered. Aleatory variability is defined as the natural randomness in a process and is supposed to be irreducible. On the contrary, epistemic uncertainty refers to the scientific uncertainty in the model of the process caused by limited data and knowledge, which can theoretically be reduced to zero with models better explaining the data. Ideally, sigma should represent the aleatory ground-motion variability obtained from repeated events on the same fault and recorded at the same station. As such, it includes only the natural randomness of the source rupture process (Anderson and Brune, 1999). Nevertheless, the computation of sigma in GMPEs is typically performed from records at multiple stations from different earthquakes, and hence mixes various paths and site responses. In other words, the variability in ground motion due to differences in paths and site response is typically considered as aleatory whereas it should be treated as epistemic uncertainty. This assumption is commonly referred to as ergodic (Anderson and Brune, 1999).

Thanks to the increasing availability of strong-motion records, several recent studies propose to refine ground-motion variability analyses by splitting sigma into various component (e.g., Chen and Tsai, 2002; Al-Atik *et al.*, 2010; Rodriguez-Marek *et al.*, 2011; Edwards and Fäh, 2013). Following the notation of Al-Atik *et al.* (2010), the total variability can then be expressed as

$$\sigma_{\text{tot}} = \sqrt{\phi^2 + \tau^2}, \tag{1}$$

in which, ϕ refers to the within-event variability (due to the variability in site conditions and path effects for a given event recorded at various stations) and τ refers to the between-event variability (essentially due to the natural source randomness). The variability σ_{tot} can further be refined by extracting the contribution of site-specific effects from ϕ, to obtain the

*German Research Centre for Geosciences (GFZ), Telegrafenberg, 14473 Potsdam, Germany; fcotton@gfz-potsdam.de.

single-station standard deviation (or single-station sigma) defined as

$$\sigma_{ss} = \sqrt{\phi_{ss}^2 + \tau^2}. \quad (2)$$

The term ϕ_{SS} is then called the event-corrected single-station sigma. A very recent work by Rodriguez-Marek *et al.* (2013) addresses the issue of the variation of single station sigma with respect to region, magnitude, and distance. First, it is remarkable from their work that the mean values of ϕ_{SS} appear to be stable (average $\phi_{SS} \approx 0.45$) across the different regions (California, Taiwan, Japan, Switzerland, and Turkey). Second, the authors observe that ϕ_{SS} depends both on magnitude and distance. They propose various models to account for such potential dependencies for moment magnitude (M_w) 4.5–8 and for distances up to 200 km, opening some new insights for improving PSHA. Nevertheless, the reliability of such models at short distances (<20 km) remains questionable due to the scarcity of near-field records of moderate-to-large events ($M_w > 6$) and potential large epistemic uncertainties associated with small event metadata (in particular depth).

The present article addresses the issue of the ground-motion variability using near-field kinematic-rupture simulations. Our strategy is to evaluate sigma from synthetic data as a function of distance. Our study focuses on the within-event component of sigma (ϕ) only. Various published kinematic source models of vertical strike-slip events are considered to represent the source process on the fault. Synthetic velocity time series are computed up to 3 Hz by convolving slip-rate functions with 1D Green's functions at stations placed at various azimuths and distances from the source. For each source model, we then extract ϕ for peak ground velocity (PGV) and study the variations of ϕ with respect to distance. It is important to note that the scope of our study is not to provide ground-motion variability values, to be directly incorporated in seismic-hazard analyses, which would require an unreasonably large number of source models and computation time. We limited our selection by considering vertical strike-slip events with $6 < M_w < 7$ only, to focus on the overall physical properties that are likely to influence the distance dependency of ϕ.

Although a variety of distance definitions are available, this work will use R_{JB}, the Joyner–Boore distance, defined as the shortest distance from the receiver to the surface projection of the fault plane (Joyner and Boore, 1981), enabling us to represent the finiteness of the fault in the region of the near-fault plane. The R_{JB} distance is equivalent to the rupture distance R_{rup} (closest distance to the rupture surface) for vertical strike-slip events, especially when the rupture is very close to the surface as for our selected fault models.

Ground-Motion Simulation

Kinematic Source Models

A total of 11 kinematic source models (i.e., the spatiotemporal distribution of slip on the fault plane), with magnitudes ranging from M_w 5.8 to 6.8, were generated for vertical strike-slip events. Eight of the source models are based on published models of past events, obtained using kinematic inversion of strong-motion observations, sometimes combined with Global Positioning System and/or Interferometric Synthetic Aperture Radar data. Although they were derived using various inversion techniques, most of them assume uniformity in rupture velocity and rise time (Table 1). These models were extracted from a database of finite-source rupture models available online (Mai and Thingbaijam, 2014; see Data and Resources). Among the eight models, six correspond to bilateral rupture and two to unilateral rupture. The classification of the models into bilateral/unilateral rupture is based on McGuire *et al.* (2002), who proposed to quantify rupture directivity using a directivity ratio (DR) computed from the second moments of the slip space–time distribution (see Appendix A). DR ranges from 0, for a 1D symmetric bilateral rupture with constant slip, to 1, for a unilateral rupture.

To properly compute ground motion up to 3 Hz, a fine grid is required to represent the slip history on the fault plane. Because the considered kinematic source models are defined on coarse grids (~2 km × 2 km), they have been interpolated on a smaller grid (e.g., 200 m × 200 m), ensuring at least five points per minimum wavelength. The interpolation procedure assumes self-similarity of the static slip beyond the Nyquist wavenumber of the original model by imposing a k^{-2} slope of the slip spectrum. The resulting numbers of subfaults are shown in Table 1.

These eight source models were complemented by three synthetic models produced using a k^{-2} description of the final slip (e.g., Causse *et al.*, 2009). The fault-plane configuration and other kinematic parameters (rise time and rupture velocity) are the same as the source model derived by Sekiguchi and Iwata (2002) for the 2000 Tottori earthquake (Table 1). The final slip on the fault plane is described in the wavenumber domain by a k^{-2} asymptotic decay beyond a corner wavenumber $k_c = K/L_c$, in which L_c is the characteristic rupture length and K is a nondimensional parameter. The parameter K expresses the degree of roughness of the slip heterogeneity. Thus we generated three source models characterized by a smooth slip distribution ($K = 0.4$), a rough one ($K = 1.6$) and an intermediate one ($K = 0.8$), so as to isolate the effect of the slip roughness on the ground-motion variability.

Source parameters and computed DRs of the eight models, extracted from the database of finite-source rupture models, are listed in Table 1. The corresponding source parameter distributions are provided in Figures 1 and 2. The images of the k^{-2} slip models are shown in Figure 3. In Table 1, magnitude (M_w) and hypocentral depth (H) of each event along with the length (L) and width (W) of the source model are given. SVF indicates the slip-velocity function considered. Each extracted model from the database was interpolated to a finer grid of subfaults, which is given by Nb. subfaults. In case of constant rupture velocity (V_R) and rise time (T_R), the corresponding values are indicated. Nb.TW refers to the number of time windows used in the inversion (Nb.TW > 1

Table 1
Information on the Kinematic Source Models from the Database

Event Name	Event Date (yyyy/mm/dd)	Author	M_w	H (km)	L (km)	W (km)	SVF	Nb. Subfaults	V_R (km/s)	Nb.TW	T_R (s)	DR
Fukuoka	2005/03/20	Asano and Iwata (2006)	6.7	14	26	18	Smooth ramp	10,248	2.1	6	3.5	0.06
Yamaguchi	1997/06/25	Miyakoshi *et al.* (2000)	5.8	8.2	16	14	Triangle	5,751	2.5	2	0.75	0.39
Kagoshimaen-hoku-seibu	1997/03/26	Horikawa (2001)	6.1	7.6	15	10	Triangle	15,251	2.5	1	0.3	0.10
Kagoshima	1997/03/26	Miyakoshi *et al.* (2000)	6.0	7.7	18	12	Triangle	14,065	2.5	2	0.75	0.36
Tottori	2000/10/06	Semmane *et al.* (2005)	6.7	14.5	32	20	Tanhyp	16,261	Variable	1	Variable	0.13
Tottori	2000/10/06	Sekiguchi and Iwata (2002)	6.8	7.8	34	17.6	Tanhyp	15,390	1.8	6	3.5	0.11
Imperial Valley	1979/10/15	Archuleta (1984)	6.5	8.0	35	13	Boxcar	211,031	Variable	1	Variable	0.95
Coyote Lake	1979/08/06	Liu and Helmberger (1983)	5.9	8.0	10	10	Triangle	10,404	2.8	1	0.5	0.60

M_w, magnitude; H, hypocentral depth; L, length; W, width of the source model; SVF, slip-velocity function; Nb. Subfaults, number of subfaults of the finer-grid fault model; V_R, rupture velocity; T_R, rise time; Nb.TW, number of time windows used in the inversion; DR, Directivity Ratio (DR $<$ 0.5 indicate bilateral and DR $>$ 0.5 indicate unilateral rupture).

in case of multi-time-window linear inversion; Hartzell and Heaton, 1983). The Kagoshimaen-hoku-seibu source model has been derived assuming constant rise time but variable rupture velocity. Nevertheless, this model has been simplified, considering an average constant rupture velocity, due to unavailability of the rupture time distribution in the source model database. The DR indicates the rupture type. Imperial Valley and Coyote Lake models (DR $>$ 0.5) can be considered as unilateral and the rest (DR $<$ 0.5) as bilateral.

Station Layout

A network of 135 hypothetical stations at various distances and azimuths was designed. The receiver configuration was set up for the R_{JB} (Joyner–Boore distance) distances 1, 3, 10, 20, 30, 60, and 100 km. We remind that R_{JB} and R_{rup} distances are the same for vertical strike-slip events with rupture reaching the surface. The receivers were positioned at the specified distances along a line parallel to the fault as well as beyond the ends of the fault extending radially outward. The locations of the stations were adapted to the respective rupture lengths of the source models. The station layout is illustrated in Figure 4 for the source model of the 2005 Fukuoka event (rupture length $L = 26$ km). The azimuth angle (θ) between the direction of the rupture propagation and the epicenter-receiver azimuth followed the definition provided in Somerville *et al.* (1997). Because we are considering strike-slip fault models only, the angle θ is measured from the epicenter to the station in the horizontal plane as illustrated in Figure 4.

Synthetic Ground-Motion Computation

Green's functions were computed considering 1D layered velocity structures (as used by the respective authors for source inversion, see Appendix B) using a discrete wavenumber technique (computer package AXITRA, Coutant, 1989). For the three synthetic k^{-2} source models, the chosen velocity structure is the one used by Sekiguchi and Iwata (2002) to derive the source model of the 2000 Tottori event. Synthetic ground motions are next computed by convolving the Green's functions with the slip history of all the subfaults, as defined in the 11 considered kinematic source models. The SVF were the same as those used by the authors. Finally three-component velocity time series were obtained at each receiver location, by summing the contributions from the different subfaults, for the respective source models. Because of the large extent of some of the faults considered in this study (number of subfaults, Table 1), the calculation of the ground motions were distributed on a computing grid to be achieved in a reasonable time. The principle of the decomposition of the computations is explained in Appendix C. The synthetics of the fault normal component from the 2005 Fukuoka model have been illustrated in Figure 5.

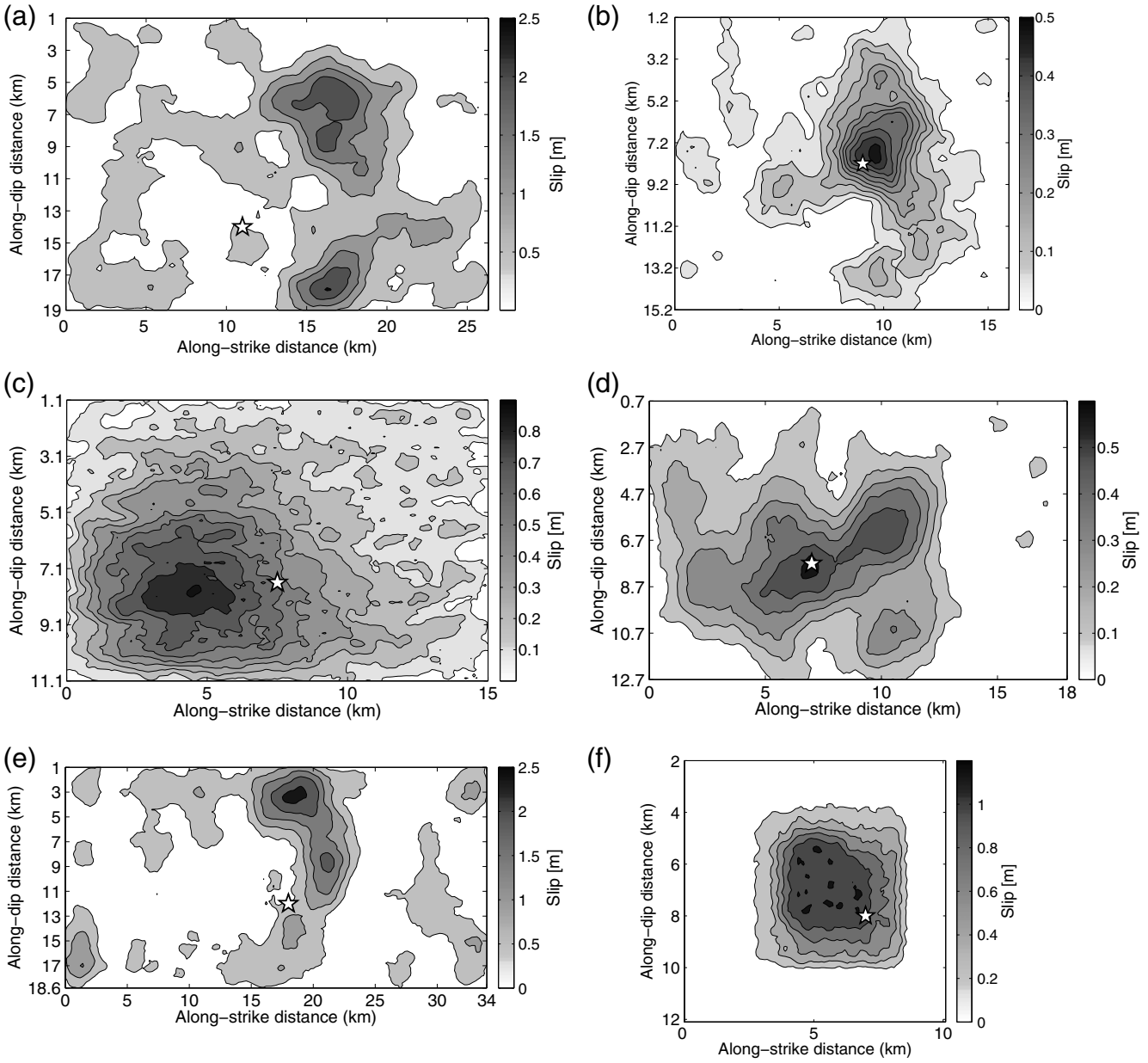

Figure 1. Slip images of the kinematic source models, having constant rupture velocity and rise time, extracted from the database of finite-source rupture models and interpolated to a finer grid. The models are (a) Fukuoka (2005), (b) Yamaguchi (1997), (c) Kagoshimaen-hoku-seibu (1997), (d) Kagoshima (1997), (e) Tottori (2000, Sekiguchi and Iwata), and (f) Coyote Lake (1979). The star symbol shows the location of the hypocenter. Contour lines represent lines of constant slip value.

PGV Calculation

We computed the PGV values as proposed by Boore *et al.* (2006), using the GMRotD50 definition. GMRotD50 is an orientation-independent geometric mean using period-dependent rotation angles. The two orthogonal components of the synthetic time series have been rotated from 1° to 90° in 1° steps, and the geometric mean for each pair of rotated time series were stored. Finally, PGV is taken as the median value of all the 90 geometric means. Ripperger *et al.* (2008) compared different PGV approximations from the two horizontal components and observed that GMRotD50 is a stable measure of the PGV showing a low dependence on the orientation of the horizontal components. Figure 6 shows the mean (with a standard deviation error bar) of ground motion in terms of natural log of PGV averaged over the different azimuths and along the R_{JB} distances for the fault models considered in this study. It is interesting to notice that in Figure 6b, the PGV values at $R_{JB} = 1$ km seems to indicate a slight reduction compared to those at $R_{JB} = 3$ km.

Analysis of PGV Within-Event Variability

We assessed the within-event component ϕ of the PGV variability (corresponding to a single source recorded at

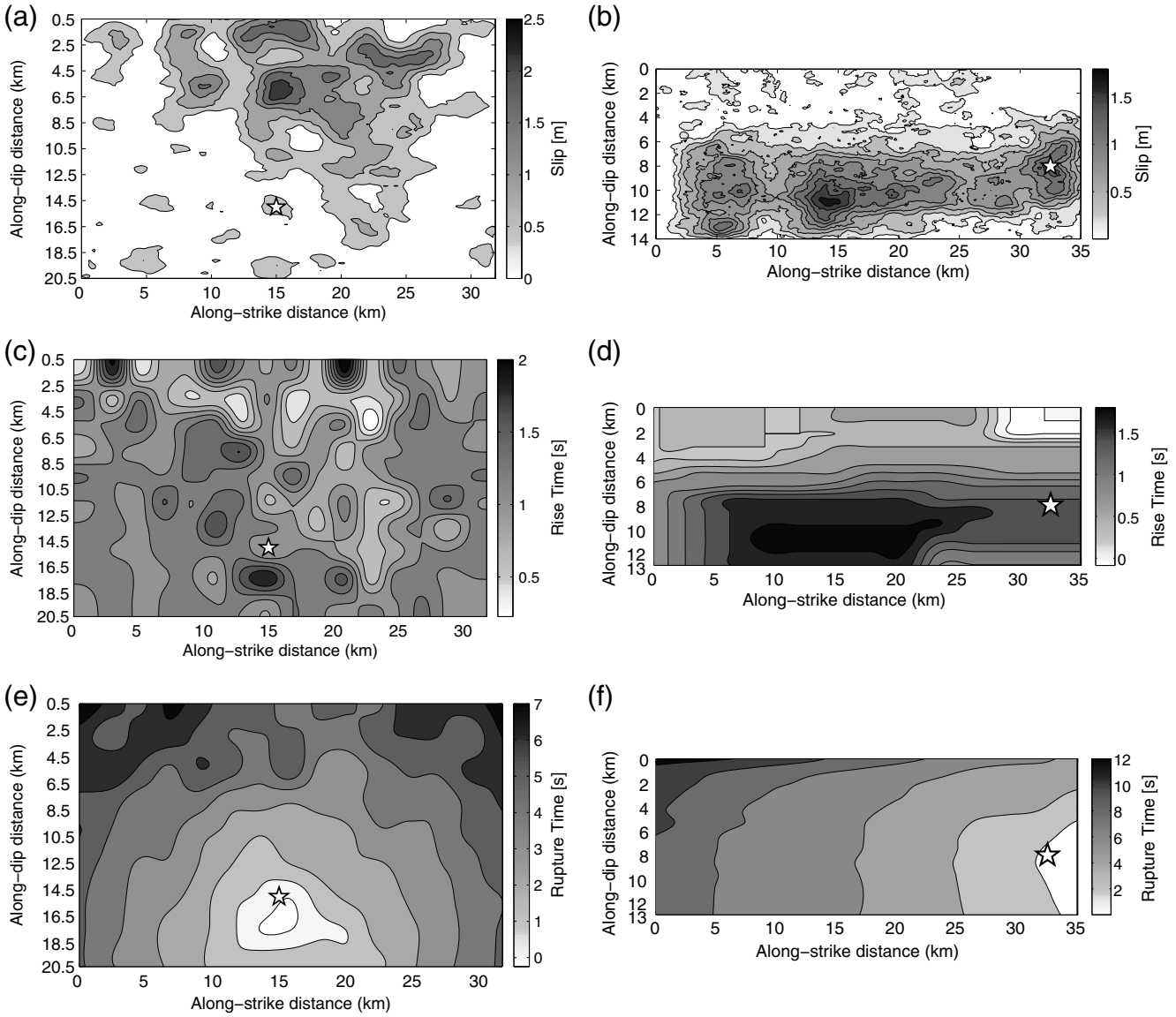

Figure 2. (a) Slip amplitude, (c) slip duration, (e) rupture front evolution images of Tottori (2000, Semmane *et al.*, 2005), and (b) slip amplitude, (d) slip duration, (f) rupture front evolution images of Imperial Valley (1979). Both kinematic source models have been extracted from the database of finite-source rupture models and then interpolated to a finer grid.

several stations) in this work. For each earthquake e, the variability at a distance R is calculated as the standard deviation of the residuals. The residuals are defined as

$$\delta_{e,R} = \ln(\mathrm{PGV})_{e,R,\theta} - \overline{\ln(\mathrm{PGV})_{\theta_{e,R}}}, \qquad (3)$$

in which $\ln(\mathrm{PGV})_{e,R,\theta}$ refers to the predictions for earthquake e at distance R and azimuth θ, and $\overline{\ln(\mathrm{PGV})_{\theta_{e,R}}}$ denotes the average over azimuths. Figure 7a illustrates the within-event ground-motion variability ϕ with varying distances for the selected source models from the finite-source rupture model database. Similarly, Figure 7b compares the variability for the three k^{-2} source models along with the two 2000 Tottori models.

We cannot ascertain any magnitude dependency of the variability due to the narrow magnitude range (M_w 5.82–6.83) considered. The most remarkable observation is that ϕ is dependent on distance. The distance dependency of ϕ exhibits two main regimes depending on the rupture type, that is, unilateral or bilateral (Fig. 7a). The perceptible trends of the PGV variability along with physical explanations on the origin of the variability are described below.

Variability Considering Bilateral Ruptures Only

We observe two main tendencies of ϕ considering bilateral rupture models only (i.e., with DR < 0.5), which could further be distinguished by the distance from the source.

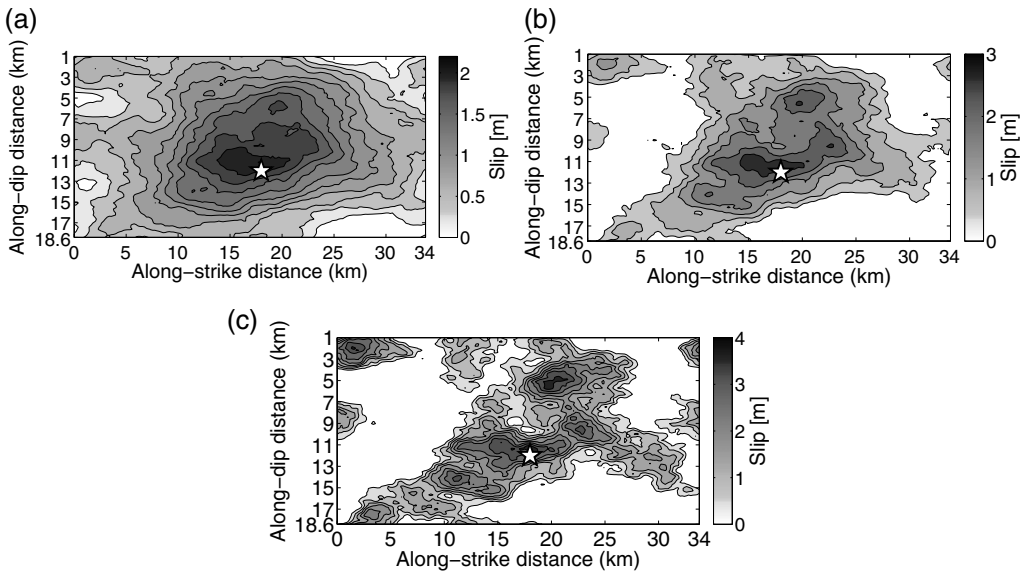

Figure 3. Slip images of the synthetic source models (a) k2-C04 (K = 0.4), (b) k2-C08 (K = 0.8), and (c) k2-C16 (K = 1.6), produced using k^{-2} descriptions of the final slip.

Variability in the Near Field (below $R_{JB} \sim 20$ km)

Considering the tendency of average values of within-event variability computed from nine bilateral models (the curve Avg-of-Bilateral-Models) in Figure 7a, variability ϕ demonstrates a fairly steady trend up to about 20 km from the source. However, the difference in the ϕ values among different rupture models is large (Fig. 8). This is because at short distances ϕ is controlled by source parameters such as location of main slip area, rupture initiation point, and hypocentral depth. A comparison of the results obtained for the Tottori event (models of Semmane *et al.*, 2005, and Sekiguchi and Iwata, 2002) and the synthetic k^{-2} source models (Fig. 7b) highlights the effect of the position of the main slip area. The source model derived for Tottori (Figs. 1e and 2a) considers the main slip area to be more widespread on the upper part in comparison to the synthetic k^{-2} source models, which assume the main slip area to be on the middle of the fault plane (Fig. 3). This may have caused the lower values of ϕ at 3 to ~20 km distance for the former models. Besides, the comparison between the three k^{-2} models (Fig. 7b) illustrates the effect of the different degrees of slip roughness (represented by the nondimensional parameter K). According to Causse *et al.* (2010), the natural variability of K can be described by a lognormal distribution with $\sigma_{\log(K)} = 0.12$. Thus, the values of K considered in our study ($K = 0.4$, $K = 0.8$, and $K = 1.6$) are expected to cover a wide range of potential degree of slip roughness ([median − 1.5 standard, median + 1.5 standard], that is ~85% of the potential values). The comparison indicates that the degree of slip roughness alone has little influence on the ground-motion variability in comparison to the position of the main slip area, except in the very near field (i.e., at 1 km), in which $\phi \sim 0.15$ for $K = 0.4$ and $\phi \sim 0.35$ for $K = 1.6$. The sensitivity to slip roughness is likely to depend on other source parameters (rise, time, and rupture velocity) and their potential correlations. For instance, large values of the rise time act as low-pass filters and could contribute to smoothing the effects of slip heterogeneities. On the other hand, shorter values of rise time (i.e., < 3.5 s) may tend to increase the sensitivity to slip roughness.

Variability in the Far Field (beyond $R_{JB} \sim 20$ km)

Interestingly, the ϕ values for the bilateral events seems to increase gradually above ~20 km distance (Fig. 7a). This tendency can be explained by the fact that in the far field extended sources behave like point sources, and accordingly, ϕ is essentially controlled by radiation pattern shape of *S* waves and Love waves. This is further investigated by analyzing the azimuth and distance dependency of the PGV values for the 2005 Fukuoka and 2000 Tottori (Semmane *et al.*, 2005) earthquakes. Figure 9a represents the PGV values at each receiver station for the respective azimuth angle θ at different R_{JB} distances. θ is the angle between the direction of rupture propagation and the epicenter-station azimuth (Somerville *et al.*, 1997). For distances larger than ~30 km, the PGV values over various azimuths along the station-array form a W-shape exhibiting radiation pattern effect. Following the *SH*-wave radiation pattern shape, we observe PGV maxima at azimuths 0°, 90°, and 180° and PGV minima at 45° and 135°. The slower decay of PGV maxima compared to that of PGV minima, with increasing distance (featuring the elongation of W-shape in Fig. 9a), eventually results in increased variability. Indeed PGV maxima are related to maximum *SH*-wave energy radiation at all distances, whereas the minima, that is, ground velocity at azimuths 45° and 135° are associated with a decrease of *SH*-wave energy radiation due to finite-source effects as distance increases.

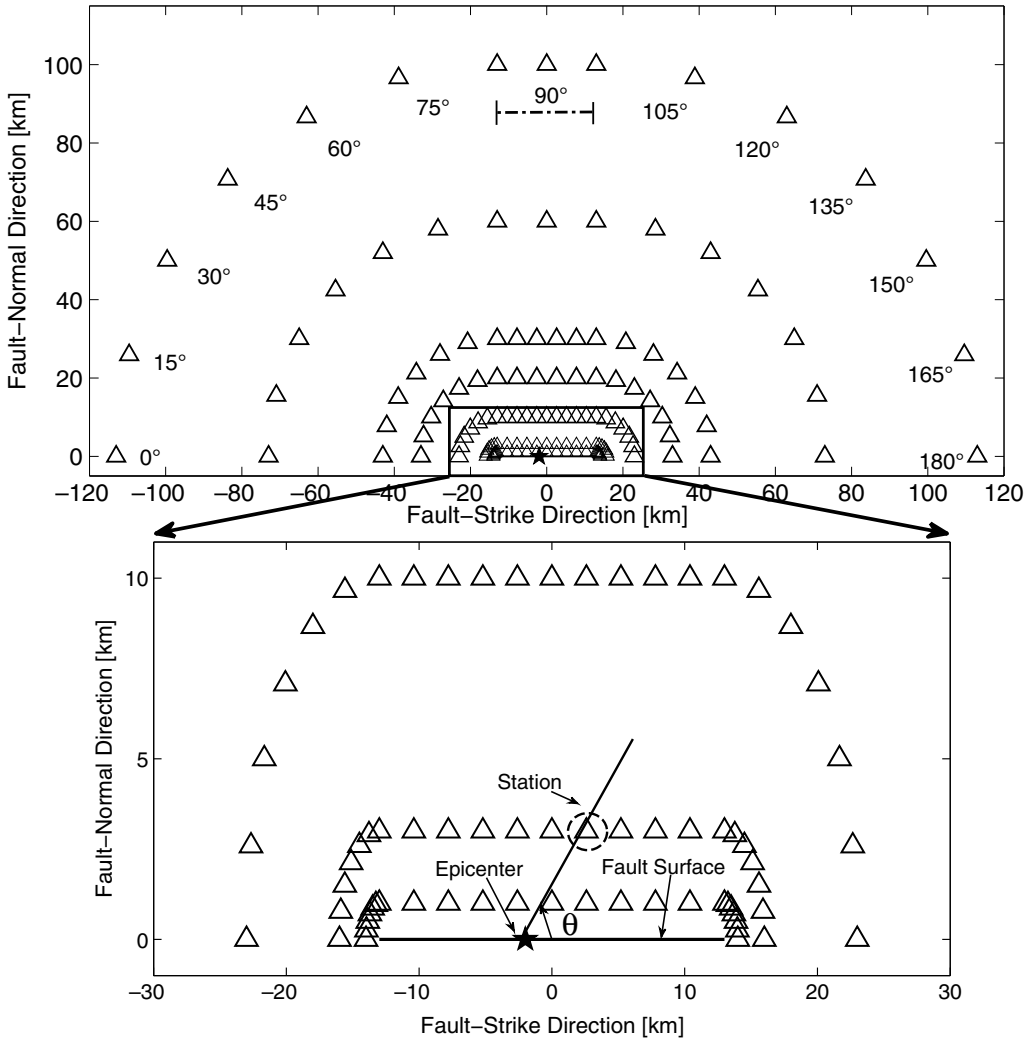

Figure 4. Station network for 2005 Fukuoka event with a zoom on the station very close to the fault (at 1, 3, and 10 km distance). The angle θ displayed on the zoomed plot represents the definition of azimuth angle between fault plane and ray path to site, according to Somerville *et al.* (1997). The radial angles (0°–180°) on the top layout represent the alignment direction of the stations at different distances, that is, the angle between the closest point on the fault and the station.

Variability Considering Unilateral Ruptures Only

Turning now to the two unilateral rupture models (i.e., with DR > 0.5) of the 1979 Imperial Valley and 1979 Coyote Lake earthquakes, we can observe that unlike the bilateral models, the variability exhibits a decreasing tendency with distance (Fig. 7a), implying higher ϕ values at shorter distances due to the presence of directivity effects. For unilateral events, strong forward-directivity effects (i.e., amplification of the PGV value) are expected for small values of the station-azimuth θ ($\theta < \sim 30°$). The dependence of directivity effects on θ is illustrated in Figure 9b, where the PGV values for the unilateral events are plotted against θ, at each R_{JB} distance. At short distances (<∼10 km) most of the stations are located in the 0°–30° azimuth region (15 out of 20 stations at 1 km) and thus associated with a strong PGV amplification due to forward-directivity effects. The large proportion of high peaked PGV values results in large variability ϕ at shorter distances. As the distance increases, fewer stations remain in the forward-directivity direction (3 out of 20 at 100 km) due to the smaller fault dimension relative to the fault-to-station distance, and hence the ϕ values decrease. At 100 km, the values of ϕ are of the same order as for bilateral events, meaning that the directivity of the rupture propagation is a second order effect far away from the source (i.e., beyond 2–3 rupture lengths).

Discussion and Conclusions

The ground-motion variability sigma is a fundamental component of PSHA studies, because small variations in sigma values can have a large influence on seismic-hazard analyses. So far GMPEs have considered sigma to be constant over distance. Though a few recent data analyses suggest that sigma is distance dependent, such studies remain, however, affected by the lack of strong-motion data recorded in the

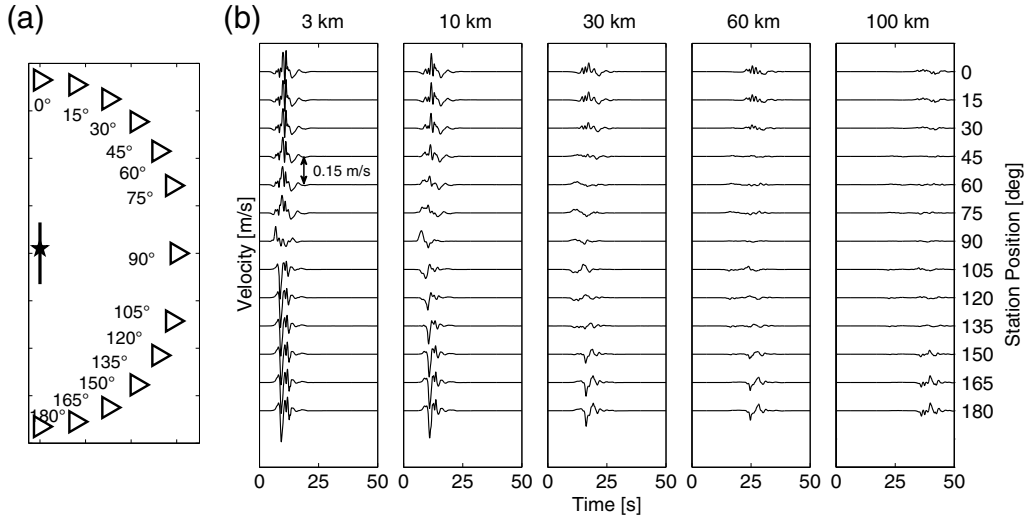

Figure 5. (a) An example of the station positions and (b) synthetic velocity time series on the fault-normal component of 2005 Fukuoka source model. Here, station position represents the station alignment (the angle between the closest point on the fault and the station) as illustrated in the station layout on the left.

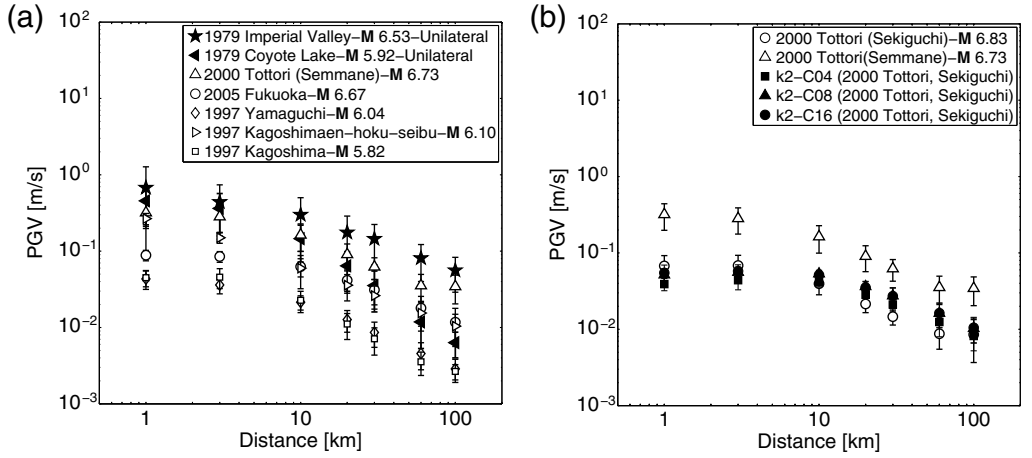

Figure 6. Mean ± standard values (bars showing one standard deviation band) of peak ground velocity (PGV) with varying R_{JB} distances for (a) source models from the finite-source rupture model database and (b) k^{-2} source models and 2000 Tottori models.

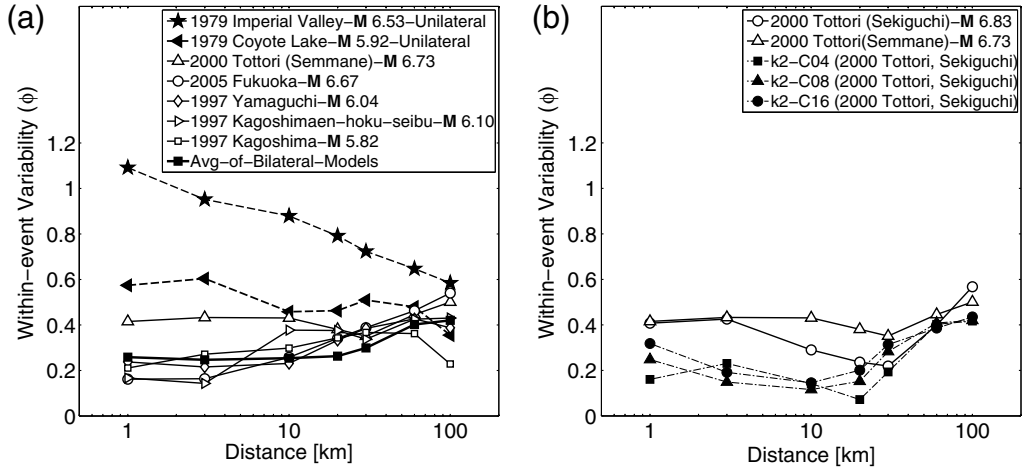

Figure 7. Within-event ground-motion variability (ϕ) with varying R_{JB} distances, for (a) source models from the finite-source rupture model database and (b) k^{-2} source models and 2000 Tottori event models.

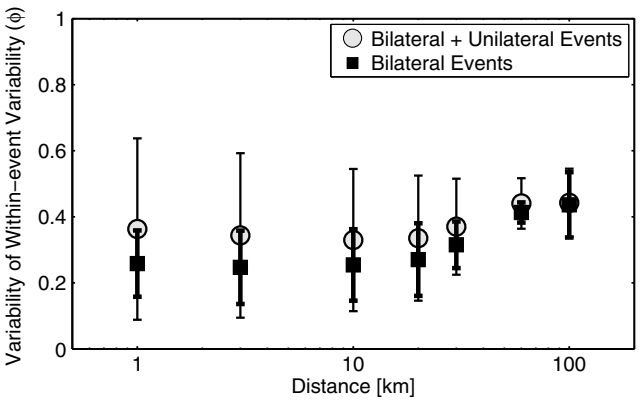

Figure 8. Mean ± standard (bars showing one standard deviation band) of the values of within-event ground-motion variability (ϕ) with varying R_{JB} distances, for the cases (1) bilateral and unilateral events combined and (2) only bilateral events.

near-source region (< 10–20 km). In this article, we have analyzed sigma from the viewpoint of simulations to complement real data studies and to investigate the influence of different source parameters on the resulting ground-motion variability. Ground motion, represented by the PGV, is computed from various kinematic source models and Green's functions computed for 1D-layered velocity models. Our study focuses on the within-event component ϕ of sigma. For simplicity, we have limited our study to vertical strike-slip faults.

Our results suggest that the within-event variability ϕ depends significantly on the rupture type, with unilateral ruptures resulting in larger ϕ values than bilateral ruptures, especially in the near-source region. Far away from the source (~100 km), this dependency vanishes and ϕ is steady ($\phi \sim 0.3$–0.5) for both kinds of ruptures. Thus the distance dependency of ϕ presents two main behaviors: (1) ϕ increases with distance for bilateral events and (2) ϕ decreases with distance for unilateral events. Interestingly, the range of within-event variability values provided by our numerical simulations in far field is consistent with the single station within-event variability (ϕ_{SS}) estimates obtained from real data by Rodriguez-Marek *et al.* (2013) ($\phi \sim 0.4$ at 100 km). It should be mentioned, however, that our ϕ estimations are not only single station but also single path because we assume a 1D velocity structure.

Using a global catalog of large shallow earthquakes, McGuire *et al.* (2002) found that approximately 80% of ruptures have DRs larger than 0.5, pointing out the overall predominance of unilateral ruptures. This shows the importance of considering directivity effects in the estimation of the between-event variability of ground motions. For a given earthquake scenario, prior knowledge about the rupture direction may contribute in refining the estimates of ϕ. The large variability, which we obtained at a short distance for unilateral ruptures, may, however, be strongly reduced if azimuth is considered as a predictor. This could be quantified by computing median ground motion from prediction models that account for directivity effects (e.g., Somerville *et al.*, 1997; Spudich and Chiou, 2008) or simply by assessing the variability in various azimuth ranges.

Our simulations are performed up to 3 Hz for simple 1D media. The ϕ values inferred in far field are essentially controlled by the shape of the wave radiation pattern. Nevertheless the radiation pattern effect, which is clearly observed in our synthetics, might be limited to lower frequency range (<~1 Hz) in real velocity structures. The theoretical four-lobe *S*-wave radiation pattern may be limited to low frequencies (< 1 Hz), with an isotropic pattern at high frequency due to the scattering of seismic waves (e.g., Liu and Helmberger, 1985; Takenaka *et al.*, 2003; Takemura *et al.*, 2009). In addition, according to Cho *et al.* (2010), observations suggest that far-field radiation patterns change from a distinct double-couple pattern, with strong directivity effects at low frequencies (< 1 Hz), to a more isotropic pattern with diminished directivity effects at high frequencies, putting forward the fact that directivity effects are also frequency dependent. This frequency dependence of directivity effects has been attributed to source incoherency by Bernard and Herrero (1994). Because our rupture models do not include any source of incoherency, the strong impact of directivity effects on the ϕ values computed from our synthetics may be weaker in the case of real earthquakes.

The results presented in this study are valid in a narrow magnitude range ($\sim 6 < M_w < \sim 7$) and for vertical strike-slip events only. In addition, due to the small number of considered source models, the source variability may be underestimated and the inclusion of additional source models may then modify the observed overall trends. Considering additional unilateral rupture models would also strengthen the conclusions on the role of directivity effects. Finally, the cogency of our results relies on the validity of the inverted source models, which may be affected by uncertainties (e.g., Mai *et al.*, 2007), due to the nonuniqueness of the inverse problem, errors in the forward model, etc. Source inversion models derived from incomplete datasets and the ground-motion prediction at a site that is not considered in the inversion can be significantly biased. This is especially true if the prediction site is isolated as pointed out by Cirella and Spudich (2013). From a set of accelerograms recorded in the area of Niigata, the authors generated thousands of good source models (i.e., with a good level of data fit) of the 2007 Chuetsu earthquake that they used to predict ground motion at the Kashiwazaki-Kariwa nuclear power plant. They found that the ground-motion scatter at the power plant is of the order of the empirically observed between-event variability. Part of this scatter arises from particular choices to parameterize the inversion process, which are inherently user dependent. For instance, two of the source models considered in our study account for variability in slip, rupture velocity, and rise time, whereas the other models assume uniformity in rupture velocity and rise time (Table 1). These *a priori* choices partially constrain distributions and correlation patterns of source parameters, which may impact the ϕ values. However, the fact that we got nearly analogous estimation of

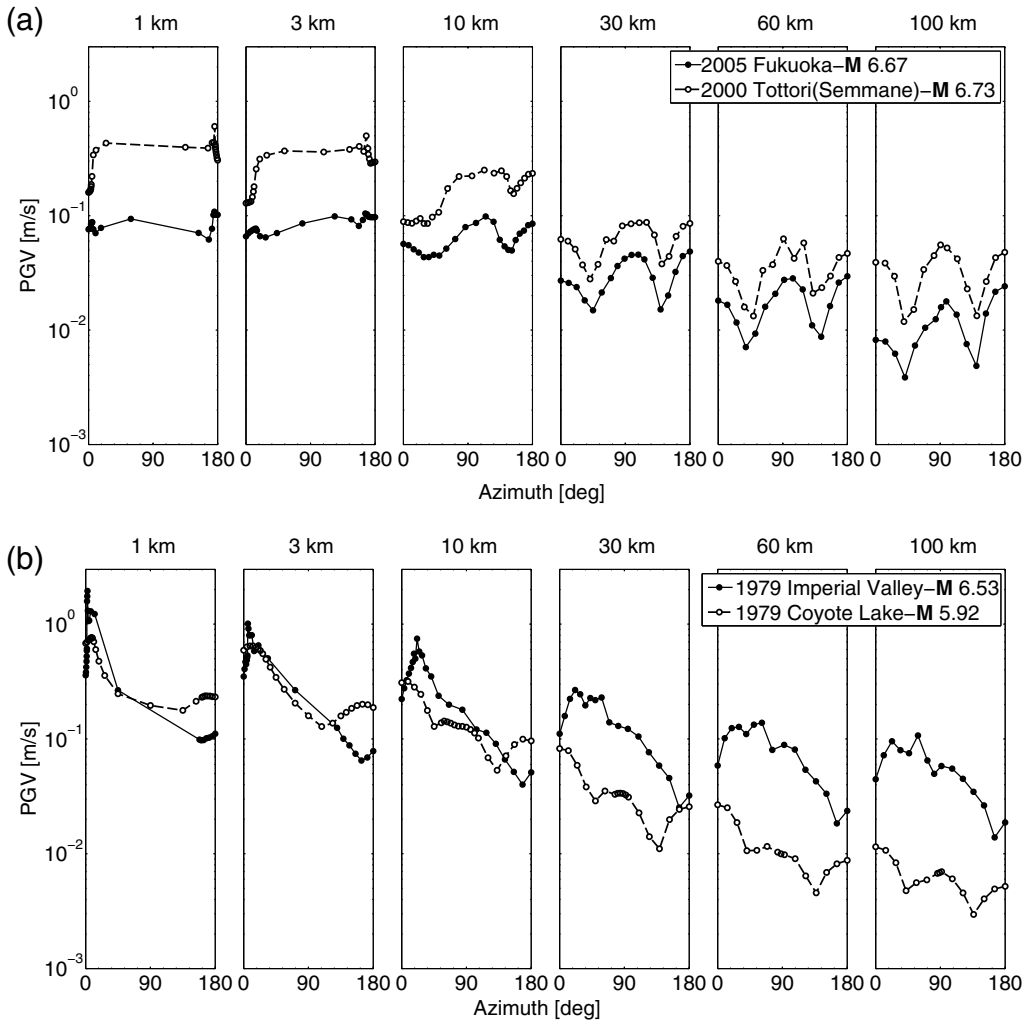

Figure 9. PGV values for the stations located at different azimuths along varying R_{JB} distances, for (a) bilateral and (b) unilateral events. Here azimuth represents θ, the angle between the epicenter and the station as illustrated in Figure 4.

ϕ from the two 2000 Tottori models, which were obtained by different authors inversion parameterization, adds credibility to our results. Furthermore, our study is intended to focus only on the variability of ground motion rather than its absolute value. The overall observed trends of the ground-motion variability have been related to global source features (rupture directivity, depth of the main slip area) that may still be captured by source inversions.

Data and Resources

The eight finite-source rupture models used in this study have been extracted from the finite-source rupture model database (Mai and Thingbaijam, 2014) available at http://equake-rc.info/SRCMOD/ (last accessed March 2014). This website is an online database of finite-fault rupture models of past earthquakes obtained using kinematic inversion of strong-motion data, sometimes combined with geodetic and/or data. The database provides the complete description of the space–time distribution of the coseismic slip, except from the model of Horikawa (2001) of the Kagoshimean-hoku-seibu event for which the rupture time distribution is not available.

Institut des Sciences de la Terre (ISTerre) is part of Labex OSUG@2020 (ANR10 LABX56). Most of the computations presented in this article were performed using the Grenoble University High Performance Computing (HPC) center, CIMENT, infrastructure (https://ciment.ujf-grenoble.fr; last accessed March 2014), which is supported by the Rhône-Alpes region (GRANT CPER07_13 CIRA: http://www.ci-ra.org; last accessed March 2014) and France-Grille (http://www.france-grilles.fr; last accessed March 2014). For the parallel computations of a large number of single jobs, we exploited the available resources of a local grid of HPC clusters (totalizing more than 3000 computing cores) in a best-effort mode, the grid middleware "cigri" (http://ciment.ujf-grenoble.fr/cigri; last accessed March 2014). The results were stored on a distributed data grid operated by the Integrated Rule-Oriented Data System (IRODS) (https://www.irods.org; last accessed March 2014).

Acknowledgments

We thank Martin Mai and an anonymous reviewer for very constructive and insightful feedback that helped us to considerably improve the article. We are thankful for the computation facilities we have been provided with from ISTerre and the Grenoble University High Performance Computing (HPC) center CIMENT.

References

Al-Atik, L., N. Abrahamson, J. J. Bommer, F. Scherbaum, F. Cotton, and N. Kuehn (2010). The variability of ground-motion prediction models and its components, *Seismol. Res. Lett.* **81,** 794–801, doi: 10.1785/gssrl.81.5.794.

Anderson, J. G., and J. N. Brune (1999). Probabilistic seismic hazard assessment without the ergodic assumption, *Seismol. Res. Lett.* **70,** no. 1, 19–28.

Archuleta, R. J. (1984). A faulting model for the 1979 Imperial Valley earthquake, *J. Geophys. Res.* **89,** no. B6, 4559–4585.

Asano, K., and T. Iwata (2006). Source process and near-source ground motions of the 2005 West Off Fukuoka Prefecture earthquake, *Earth Planet Space* **58,** 93–98.

Bernard, P., and A. Herrero (1994). Slip heterogeneity, body-wave spectra, and directivity of earthquake ruptures, *Ann. Geofisc.* **XXXVII,** 1679–1690.

Bommer, J. J., and N. A. Abrahamson (2006). Why do modern probabilistic seismic-hazard analyses often lead to increased hazard estimates? *Bull. Seismol. Soc. Am.* **96,** 1967–1977.

Boore, D. M., J. W. Lamprey, and N. A. Abrahamson (2006). Orientation-independent measures of ground motion, *Bull. Seismol. Soc. Am.* **96,** no. 4A, 1502–1511, doi: 10.1785/0120050209.

Bouchon, M. (1981). A simple method to calculate Green's functions for elastic layered media, *Bull. Seismol. Soc. Am.* **71,** no. 4, 959–971.

Causse, M., E. Chaljub, F. Cotton, C. Cornou, and P. Y. Bard (2009). New approach for coupling k-2 and empirical Green's functions: Application to the blind prediction of broadband ground-motion in the Grenoble basin, *Geophys. J. Int.* **179,** 1627–1644.

Causse, M., F. Cotton, and M. Mai (2010). Constraining the roughness degree of slip heterogeneity, *J. Geophys. Res.* doi: 10.1029/2009JB006747.

Chen, Y.-H., and C.-C. P. Tsai (2002). A new method for estimation of the attenuation relationship with variance components, *Bull. Seismol. Soc. Am.* **92,** no. 5, 1984–1991.

Cho, H., J. Hu, Y. Klinger, and E. M. Dunham (2010). Frequency dependence of radiation patterns and directivity effects in ground motion from earthquakes on rough faults, *Eos Trans. AGU*, (Fall Meet.), Abstract #S51A-1914.

Cirella, A., and P. Spudich (2013). Aleatory and epistemic uncertainties in interpolated ground motions—Example from the Kashiwazaki-Kariwa Nuclear Powaer Plant recordings of the July 16, 2007, Niigata-ken Chuetsu-oki, Japan, earthquake, *Geophys. Res. Abstr.*, EGU2013-5932.

Coutant, O. (1989). Program of numerical Simulation AXITRA, *Research Reports LGIT*, Université Joseph Fourier, Grenoble (in French).

Edwards, B., and D. Fäh (2013). A stochastic ground motion model for Switzerland, *Bull. Seismol. Soc. Am.* **103,** doi: 10.1785/0120110331.

Hartzell, S. H., and T. H. Heaton (1983). Inversion of strong ground motion and teleseismic waveform data for the fault rupture history of the 1979 Imperial Valley, California, earthquake, *Bull. Seismol. Soc. Am.* **73,** 1553–1583.

Horikawa, H. (2001). Earthquake doublet in Kagoshima, Japan: Rupture of asperities in a stress shadow, *Bull. Seismol. Soc. Am.* **91,** no. 1, 112–127.

Joyner, W. B., and D. M. Boore (1981). Peak horizontal acceleration and velocity from strong-motion records including records from the 1979 Imperial Valley, California, earthquake, *Bull. Seismol. Soc. Am.* **71,** no. 6, 2011–2038.

Liu, H., and D. V. Helmberger (1983). The near-source ground motion of the 6 August 1979 Coyote Lake, California, earthquake, *Bull. Seismol. Soc. Am.* **73,** no. 1, 201–218.

Liu, H., and D. V. Helmberger (1985). The 23:19 aftershock of the 15 October 1979 Imperial valley earthquake: More evidence for an asperity, *Bull. Seismol. Soc. Am.* **75,** 689–708.

Mai, P. M., and K. K. S. Thingbaijam (2014). SRCMOD: An online database of finite-fault rupture models, *Seismol. Res. Lett.* **85,** no. 6, doi: 10.1785/0220140077.

Mai, P. M., J. Burjanek, B. Delouis, G. Festa, C. Francois-Holden, D. Monelli, T. Uchide, and J. Zahradnik (2007). Source-inversion blind test: Initial results and further developments, *Eos Trans. AGU*, **88,** no. 52 (Fall Meet. Suppl.), Abstract S53C-08.

McGuire, J. J., L. Zhao, and T. H. Jordan (2002). Predominance of unilateral rupture for a global catalog of large earthquakes, *Bull. Seismol. Soc. Am.* **92,** no. 8, 3309–3317.

Miyakoshi, K., T. Kagawa, H. Sekiguchi, T. Iwata, and K. Irikura (2000). Source characterization of inland earthquakes in Japan using source inversion results, Paper read at *Proc. 12th World Conf. Earthq. Eng.*, Auckland, New-Zealand, 30 January–4 February 2000.

Ripperger, J., P. M. Mai, and J.-P. Ampuero (2008). Variability of near-field ground motion from dynamic earthquake rupture simulations, *Bull. Seismol. Soc. Am.* **98,** no. 3, 1207–1228, doi: 10.1785/0120070076.

Rodriguez-Marek, A., F. Cotton, N. Abrahamson, S. Akkar, L. Al-Atik, B. Edwards, G. Montalva, and M. Dawood (2013). A model for single-station standard deviation using data from various tectonic regions, *Bull. Seismol. Soc. Am.* **103,** 3149–3163, doi: 10.1785/0120130030.

Rodriguez-Marek, A., G. A. Montalva, F. Cotton, and F. Bonilla (2011). Analysis of single-station standard deviation using the KiK-net data, *Bull. Seismol. Soc. Am.* **101,** 1242–1258, doi: 10.1785/0120100252.

Sekiguchi, H., and T. Iwata (2002). Source process and near-fault ground motion of the 2000 Tottori-ken Seibu earthquake, *Monthly Chikyu* no. 38, 182–188 (in Japanese).

Semmane, F., F. Cotton, and M. Campillo (2005). The 2000 Tottori earthquake: A shallow earthquake with no surface rupture and slip properties controlled by depth, *J. Geophys. Res.* **110,** no. B3, B03306, doi: 10.1029/2004JB003194.

Somerville, P. G., N. F. Smith, R. W. Graves, and N. A. Abrahamson (1997). Modification of empirical strong ground motion attenuation relations to include the amplitude and duration effects of rupture directivity, *Seismol. Res. Lett.* **68,** 199–222.

Spudich, P., and B. S.-J. Chiou (2008). Directivity in NGA earthquake ground motion: Analysis using isochrone theory, *Earth. Spectra* **25,** 279–298.

Takemura, S., T. Furumura, and T. Saito (2009). Distortion of the apparent *S*-wave radiation pattern in the high-frequency wavefield: Tottori-Ken Seibu, Japan, earthquake of 2000, *Geophys. J. Int.* **178,** 950–961.

Takenaka, H., Y. Mamada, and H. Futamure (2003). Near-source effect on radiation pattern of high-frequency *S* waves: Strong *SH-SV* mixing observed from aftershocks of the 1997 northwestern Kagoshima, Japan, earthquakes, *Phys. Earth Planet. In.* **137,** nos. 1/4, 31–43.

Appendix A

Computation of Directivity Ratios

For each source model, we compute the directivity ratio (DR) as proposed by McGuire *et al.* (2002). From the space–time slip distribution, we first compute the second spatial moment $\hat{\mu}^{(2,0)}$, the second temporal moment $\hat{\mu}^{(0,2)}$, and the mixed moment $\hat{\mu}^{(1,1)}$ defined as

$$\hat{\mu}^{(2,0)} = \iint \dot{f}(\vec{r},t)(\vec{r}-\vec{r}_0)(\vec{r}-\vec{r}_0)^T dV dt, \qquad \text{(A1)}$$

$$\hat{\mu}^{(0,2)} = \iint \dot{f}(\vec{r},t)(t-t_0)^2 dV dt, \qquad \text{(A2)}$$

and

$$\hat{\mu}^{(1,1)} = \iint \dot{f}(\vec{r}, t)(\vec{r} - \vec{r}_0)(t - t_0)dVdt, \tag{A3}$$

in which $\dot{f}(\vec{r}, t)$ is the space–time moment rate function, and $\vec{r}_0$ and t_0 refer to the spatial and temporal centroids.

Next, we determine the characteristic duration, expressed as

$$\tau_c = 2\sqrt{\hat{\mu}^{(0,2)}/M_0)} \tag{A4}$$

and the characteristic dimension in a direction $\vec{n}$, expressed as

$$x_c(\vec{n}) = 2\sqrt{\vec{n}^T(\hat{\mu}^{(2,0)}/M_0)\vec{n}}, \tag{A5}$$

in which M_0 denotes the seismic moment. The characteristic rupture length L_c is defined as $x_c(\vec{n}_1)$, the maximum value of $x_c(\vec{n})$, $\vec{n}_1$ being the Eigen vector associated with the largest eigen value. The ratio

$$\nu_c = L_c/\tau_c \tag{A6}$$

then represents the characteristic rupture velocity.

Finally, we compute the average velocity of the instantaneous spatial centroid:

$$\nu_0 = \hat{\mu}^{(1,1)}/\hat{\mu}^{(0,2)}. \tag{A7}$$

The DR is defined as the ratio ν_0/ν_c.

Appendix B

Velocity Models Used for Ground-Motion Computation

All the considered velocity models are the ones that have been used to perform source inversions, except the Imperial Valley earthquake, for which the model has been slightly simplified to reduce computation time. The velocity models considered in the ground-motion simulation are given in Table B1 for the bilateral models and in Tables B2 and B3 for unilateral models; V_P, V_S indicate the velocity and Q_P, Q_S the quality factor of P and S waves, respectively. D indicates density of the material in the layer.

For the Imperial Valley (1979) event, Archuleta (1984) assumes a model with velocity gradient as presented in Table B2. For the Green's function computation with Axitra program, different sublayers of the given velocity model were considered, which involved linear interpolation of the values. For example, the second layer (between 0.4 and 5 km) was divided into $N = 5$ sublayers of thickness $dh = 1150$ m each, and values of the other parameters were taken at the middle of each sublayer. Similarly, the third layer (between 5 and 11 km depth) was divided into $N = 6$ sublayers of thickness $dh = 1000$ m. The fourth layer (between 11 and 11.1 km) marks the discontinuity. Finally, the fifth layer (between 11.1 and 12 km depth) was divided into $N = 2$ sublayers of thickness $dh = 450$ m. The final velocity model adopted is given in Table B3.

Table B1
Velocity Models of the Bilateral Events

Event Name	Depth (m)	V_P (m/s)	V_S (m/s)	D (kg/m^3)	Q_P	Q_S
Fukuoka	0	5500	3200	2600	∞	∞
(2005)	5000	6000	3460	2700	∞	∞
	18000	6700	3870	2800	∞	∞
Yamaguchi	0	5600	3300	2600	400	400
(1997)	3000	6000	3500	2700	450	450
	30000	6600	3800	2900	500	500
Kagoshimaen-	0	2800	1620	2100	80	40
hoku-seibu	500	4900	2830	2300	300	150
(1997)	5000	6000	3460	2700	300	150
	15000	6700	3870	3100	500	250
	35000	7800	4500	3400	1000	500
Kagoshima	0	3100	1800	2300	200	200
(1997)	500	4400	2500	2500	350	350
	3000	5900	3400	2700	450	450
	22000	7000	4000	3000	500	500
Tottori (2000,	0	5500	3180	2600	500	200
Semmane	2000	6050	3490	2700	500	200
et al., 2005)	16000	6600	3810	2800	200	200
	38000	8030	4620	3100	500	200
Tottori (2000,	0	5500	3179	2600	500	200
Sekiguchi	2000	6050	3497	2700	500	200
and Iwata,	16000	6600	3815	2800	500	200
2002)	38000	8000	4600	3000	500	200
	20000	8100	4620	3300	500	200

Table B2
Initial Velocity Model of Imperial Valley (1979) from Database

Event Name	Depth (m)	V_P (m/s)	V_S (m/s)	D (kg/m^3)	Q_P	Q_S
Imperial Valley (1979),	0	1700	400	1800	∞	∞
Initial Model	400	1800	700	1800	∞	∞
	5000	5650	3200	2500	∞	∞
	11000	5850	3300	2800	∞	∞
	11100	6600	3700	2800	∞	∞
	12000	7200	4150	2800	∞	∞

Appendix C

Computations of the Synthetic Ground Motions for Large Faults

The principle of the decomposition of the computations of ground motions for the large faults considered in this study is as follows:

Let F stand for one of those faults. F is further decomposed into N_s subfaults, such that the typical length of each subfault is a fifth of the minimum wavelength on F. Let N_r

Table B3
Velocity Models of the Unilateral Events

Event Name	Depth (m)	V_P (m/s)	V_S (m/s)	D (kg/m^3)	Q_P	Q_S
Imperial Valley	0	1700	400	1800	∞	∞
(1979),	400	1800	700	1800	∞	∞
Interpolated Model	1550	2281	1013	1888	∞	∞
	2700	3243	1638	2063	∞	∞
	3850	4206	2263	2238	∞	∞
	5000	5169	2888	2413	∞	∞
	6000	5667	3208	2525	∞	∞
	7000	5700	3225	2575	∞	∞
	8000	5733	3242	2625	∞	∞
	9000	5767	3258	2675	∞	∞
	10000	5800	3275	2725	∞	∞
	11000	5833	3292	2775	∞	∞
	11100	6225	3500	2800	∞	∞
	11550	6750	3813	2800	∞	∞
	12000	7050	4038	2800	∞	∞
Coyote Lake (1979)	0	3000	1500	2400	∞	∞
	500	5000	2800	2700	∞	∞
	3000	5700	3300	2780	∞	∞
	12000	6900	3300	3000	∞	∞
	60000	8100	4670	3200	∞	∞

(here $N_r = 135$) be the number of receivers, then the computation of the ground motions is done in three steps: (1) the components of all Green's functions relating the N_s subfaults to the N_r receivers are computed with the Axitra code (Coutant, 1989); (2) each Green's function is convolved in space and time to account both for the magnitude and focal mechanism of the subfault and for the imposed rupture kinematics; and (3) the contributions of the N_s subfaults are summed at each of the N_r receivers.

The $N_s \times N_r$ calculations needed by step (1) were done in parallel on the number of subfaults, that is, for each subfault the calculations at all receivers were gathered in a single job. For this purpose, we exploited the available resources of a local grid of High Performance Computing clusters (totalizing more than 3000 computing cores) in a best-effort mode thanks to the grid middleware "cigri." The results, consisting of one binary file per subfault, were stored on a distributed data grid operated by the IRODS system. The convolutions needed by step (2) were also distributed on the computing grid and stored again on the data grid. Finally, the reduce operation needed in step (3) was done for all receivers by successive grouping of the sources by packets, the size of which was controlled by the maximum number of binary files that would fit in the random access memory (RAM) of each computing node. For the example of the Imperial Valley calculations, each binary file containing the contribution of a single subfault at all receivers was about 16 MB, and the size of the source packets was 200 so that the summation could be done in a RAM of size 4 GB. For this event, which was the most demanding of all cases, the total time needed to compute the Green's functions was about 4000 hours of a single CPU core on an Intel E5-2670 with frequency 2.6 GHz.

Institut des Sciences de la Terre (ISTerre)
University Grenoble Alpes/CNRS/IRD/IFSTTAR
F-38000 Grenoble, France
afifa.imtiaz@ujf-grenoble.fr
mathieu.causse@ujf-grenoble.fr
emmanuel.chaljub@ujf-grenoble.fr
fabrice.cotton@ujf-grenoble

Manuscript received 16 April 2014;
Published Online 27 January 2015